ACS SENSORS

pubs.acs.org/acssensors Article

mRNA Display Pipeline for Protein Biosensor Construction

Zhenling Cui, Cagla Ergun Ayva, Yi Jin Liew, Zhong Guo, Roxane Mutschler, Birgit Dreier, Maria M Fiorito, Patricia Walden, Christopher B Howard, Fernanda Ely, Andreas Plückthun, Carel Pretorius, Jacobus PJ Ungerer, Ashley M Buckle, and Kirill Alexandrov*

Cite This: *ACS Sens.* 2024, 9, 2846−2857 Read Online

ACCESS | Metrics & More | Article Recommendations | Supporting Information

ABSTRACT: Despite the significant potential of protein biosensors, their construction remains a trial-and-error process. The most obvious approach for addressing this is to utilize modular biosensor architectures where specificity-conferring modalities can be readily generated to recognize new targets. Toward this goal, we established a workflow that uses mRNA display-based selection of hyper-stable monobody domains for the target of choice or ribosome display to select equally stable DARPins. These binders were integrated into a two-component allosteric biosensor architecture based on a calmodulin-reporter chimera. This workflow was tested by developing biosensors for liver toxicity markers such as cytosolic aspartate aminotransferase, mitochondrial aspartate aminotransferase, and alanine aminotransferase 1. We demonstrate that our pipeline consistently produced >10^3 unique binders for each target within a week. Our analysis revealed that the affinity of the binders for their targets was not a direct predictor of the binder's performance in a biosensor context. The interactions between the binding domains and the reporter module affect the biosensor activity and the dynamic range. We conclude that following binding domain selection, the multiplexed biosensor assembly and prototyping appear to be the most promising approach for identifying biosensors with the desired properties.

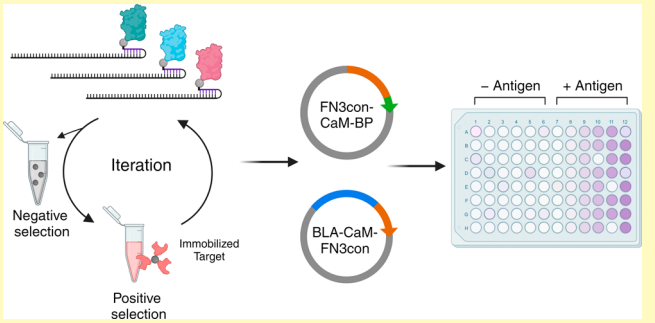

KEYWORDS: *protein biosensor, mRNA display, Monobodies, DARPins, synthetic protein binding domain*

Protein switches are ubiquitous and essential in biological signaling systems where they enable cells to sense and respond to diverse molecular signals in real time.[1] The biological importance of protein switches sparked attempts to develop artificial versions with customizable inputs and outputs. Such switches, also known as protein biosensors, became invaluable research tools in cell-, neuro-, and synthetic biology and may have important clinical applications.[2−4] Development of protein biosensors requires creation of an OFF (or less frequently ON) state of a reporter protein that can be reversed by the analyte of choice.[2,4−6]

Biosensor architectures can be divided into two main classes: fully integrated systems,[4,7,8] which are controlled by a ligand-induced conformational change, and multicomponent systems,[9−13] where the ligand modulates local concentrations and interactions of the components. The latter architectures are more modular and, in the simplest configuration, embodied by split systems where the ligand brings two parts of a reporter into proximity.[12,13] More advanced versions of two-component systems are based on autoinhibited reporters such as proteases or luciferases that are activated through proteolysis or sterically regulated activator binding.[11,14] A recent example of the latter includes a caged split luciferase fragment that is uncaged upon binding to its target. This binding enables the association of the complementary split luciferase fragment, thereby reconstituting the enzyme's activity.[11] However, due to the requirement for steric competition, this biosensor architecture is suitable only for large analytes.

We previously reported an alternative approach where two- and three-component biosensor architectures utilize a chimera of calmodulin with a reporter domain that is activated by a calmodulin-binding peptide (CaM-BP) (Figure 1A).[9,15] The local concentration of CaM-BP is regulated by the analyte-mediated scaffolding of the components, leading to fluorescent, luminescent, colorimetric, or electrochemical outputs. This platform was used to create biosensors of ions, small molecules, and proteins that demonstrated large dynamic ranges and fast response.[15]

These advancements shifted our focus from biosensor architecture design to the development of methodologies for fast construction of new biosensors. The latter requires an efficient process for the development of binding domains that

Received: November 20, 2023
Revised: May 1, 2024
Accepted: May 21, 2024
Published: May 29, 2024

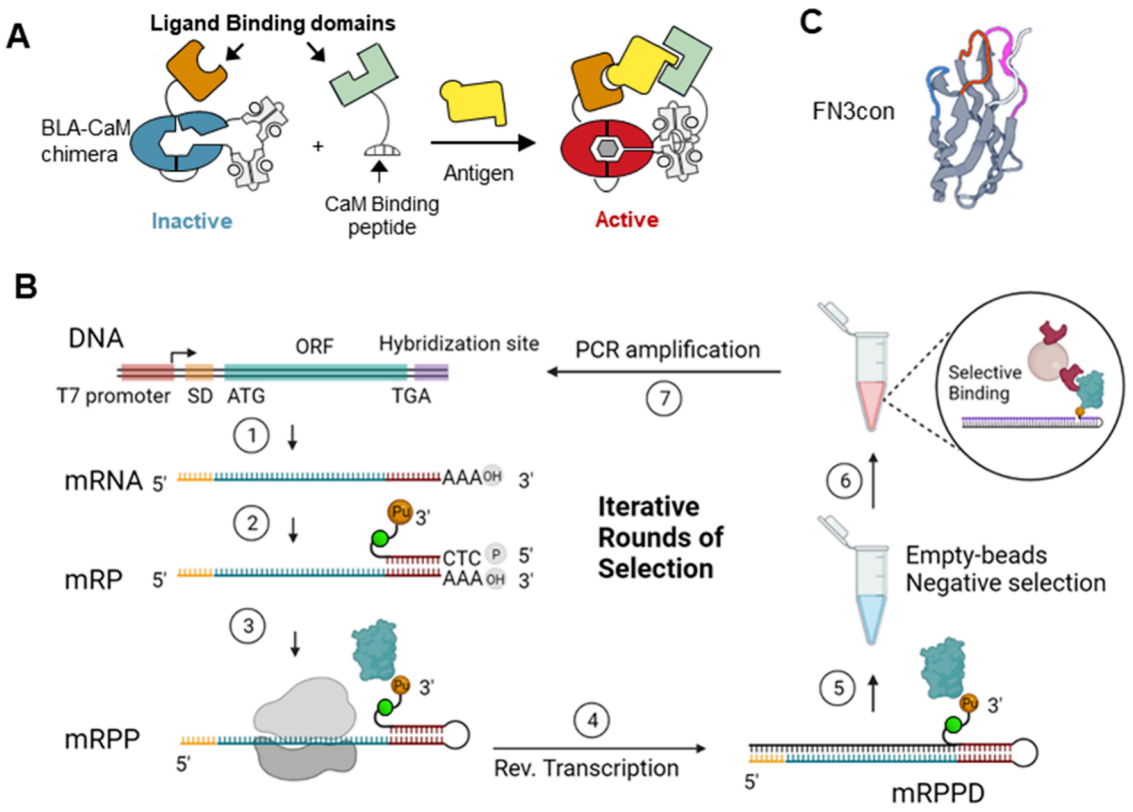

Figure 1. Application of mRNA display to protein biosensor development. (A) Schematic representation of a two-component biosensor based on a β-lactamase:calmodulin chimera. Association of the marked ligand-binding domains with the target leads to the assembly of the biosensor complex's activation leading to hydrolysis of the β-lactamase reporter substrate represented by the hexagon. (B) Flowchart of the optimized mRNA display starting from a linear DNA library containing transcription and translation initiation elements in the 5′-UTR, followed by a Flag tag, a FN3 coding sequence, a flexible linker, a TGA stop codon, and an oligonucleotide hybridization site at 3′-UTR. These templates are used to generate an mRNA library by *in vitro* transcription (step 1), followed by the conjugation of a PuL (step 2). The green circle indicates the fluorescein dT in the linker region of PuL. The translating ribosome stalls at the stop codon in the absence of release factors and promotes the formation of a covalent bond between puromycin on mRNA and the nascent polypeptide chain (step 3). Following reverse transcription (step 4), EDTA is added to the reaction mixture, and the library of conjugates is subjected to negative selection against the matrix (step 5) and then to positive selection against the immobilized target colored in red (step 6). Selected genes are amplified by PCR (step 7) and used in the next selection round. (C) Ribbon representation of the FN3con protein domain with highlighted CDR1 (blue), CDR2 (orange), and CDR3 (magenta) loops that are randomized in our library.

can simultaneously and selectively associate with an analyte, bringing biosensor components into proximity. To this end, we sought a method that allows rapid development of high-affinity binding domains, even for targets with unknown three-dimensional structures. Numerous *in vivo* (bacteria, yeast, phage, etc.)[16] and *in vitro* display (ribosome display, mRNA display, DNA display)[17] systems can create a linkage between genotype and phenotype, thereby enabling the selection and identification of binding domains. Among these, mRNA display, which relies on a puromycin molecule that mimics amino-acylated tRNA and forms a stable amide bond with nascent polypeptides, has numerous advantages.[18] It supports large libraries (up to 10^{13} variants) and allows an extensive exploration of sequence space while offering flexibility in the choice of buffer conditions and operational temperatures. Further, mRNA display is significantly faster than the selection systems involving cells, such as phage and yeast display. For example, a single selection round of mRNA display can be completed in a day while phage display selection cycle takes closer to a week. Similarly, ribosome display, where the folded protein and the encoding mRNA remain connected through the ribosome, has been routinely used to obtain high affinity binders from equally large libraries, limited only by the number of ribosomes in the reaction (typically 10^{12}).[19]

On the other hand, mRNA display is a multistep procedure that requires meticulous quality control of individual steps and, as a result, only established in a few laboratories.[20] High diversity of libraries used for mRNA display also contain more nonfunctional sequences that must be removed in the selection process. As a result, mRNA display typically involves 4 to 10 rounds of selection, while phage display generally requires 3−5 rounds, while ribosome display is often carried out over 4 rounds. The inclusion of more selection cycles means a longer processing time, higher potential for contamination, and an elevated risk of selection failure. Despite these potential pitfalls, mRNA display has been successfully used to select high-affinity and selective binders from libraries of nanobodies, SH3 domains, Fab domains, ScFv, and fibronectin domains.[21−24] Therefore, we chose to utilize mRNA display in conjunction with a synthetic library of stabilized FN3 monobody domains as an input platform for biosensors development. For comparison, we have selected DARPins for one of the targets with a ribosome display.

https://doi.org/10.1021/acssensors.3c02471
ACS Sens. 2024, 9, 2846−2857

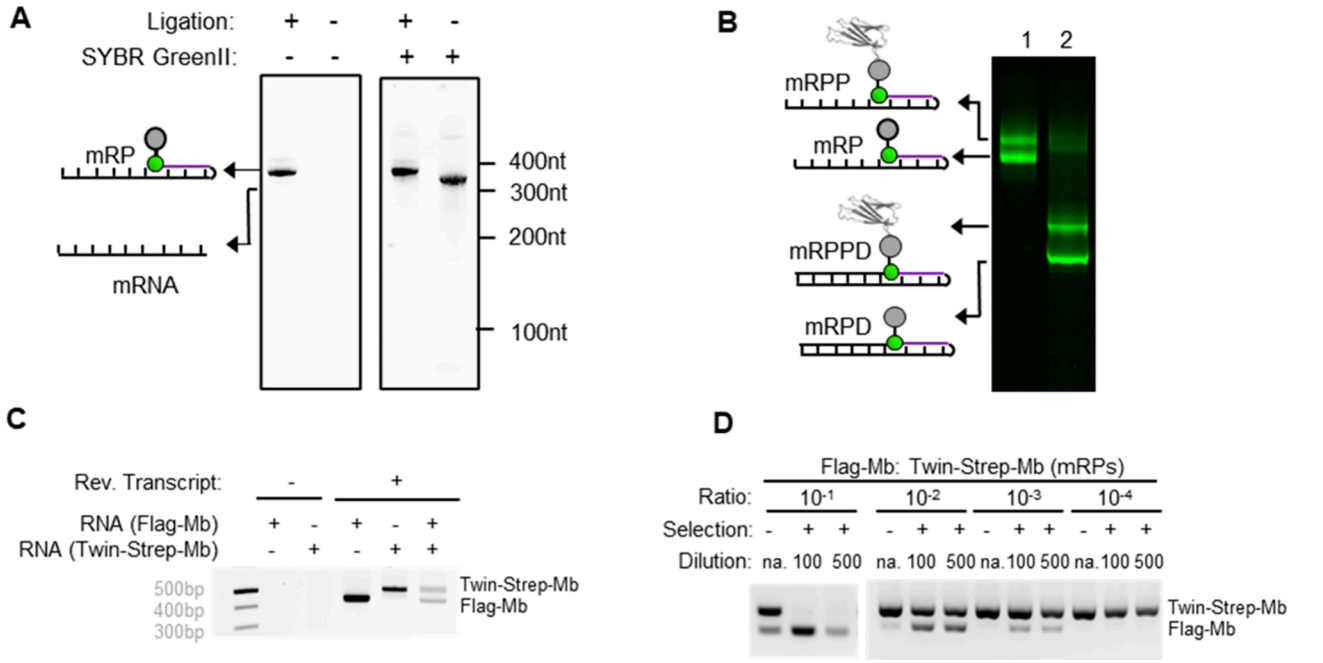

Figure 2. Optimization of the mRNA display protocol and evaluation of its enrichment capacity by selecting a Flag-tagged monobody from a mixture with a Twin-strep-tagged monobody against an anti-Flag antibody. (A) Picture of a 6% TBE-urea gel loaded with a representative mRNA and fluorescent mRNA-puromycin conjugate. The left panel shows conjugated mRNA-puromycin (mRP) detected by fluorescence scanning, with mRNA being invisible. The right panel shows the same gel stained with SYBR GreenII, visualizing both mRNA and mRP bands. (B) *In vitro* translation of the mRP (lane 1) followed by reverse transcription (lane 2). The samples were separated on a 4−12% NuPAGE gel and scanned for fluorescence. By comparing the upper and lower bands in each lane, we estimated that approximately 40% of mRNA was conjugated to protein, implying that ~10^{13} molecules were displayed in our round 1 selection starting from 10^{14} mRNA molecules (100 pmol). We observed faster mobility of cDNA-mRNA hybrids compared to their mRNA templates, possibly due to their distinct topologies. (C) Design of two RNA constructs with comparable reverse transcription and PCR amplification efficiencies. We designed two mRNAs with a Flag-tag and a Twin-Strep-tag in front of a monobody protein (PDB: 1TTF). The individual mRNA or a 1:1 mixture of the two mRNAs was reverse transcribed, PCR amplified, and separated on an agarose gel. The negative controls of two mRNAs without reverse transcription did not yield PCR amplicons, indicating the absence of a dsDNA template carryover. D. Selection results of Flag-monobody mRNA. The mRP conjugates of Flag- and Twin-Strep-tag constructs were mixed at 1:10, 1:100, 1:1000, and 1:10000 ratios, and 1 μM of the mixture was subjected to translation and selection. The eluted cDNA was subsequently diluted at the specified ratio, PCR-amplified, and visualized on the agarose gel.

Here, we report the establishment of an mRNA display binder selection platform and its application to the development of biosensors of protein markers for liver toxicity.

RESULTS

Establishing an mRNA Display Pipeline Based on the PURE *In Vitro* Translation System. mRNA display provides a linkage between genotype (nucleic acid) and phenotype (protein) through a puromycin molecule.[25] Several strategies for conjugating the puromycin oligonucleotide linker (PuL) with mRNA transcripts were reported, including Y ligation,[26] UV cross-linking,[27] split ligation,[21] and noncovalent linkage termed TRAP.[28] Among these, TRAP display stands out as the fastest display system allowing completing six rounds of selection within only 14 h. However, it relies on hybridization between the PuL and mRNA transcripts, which are expected to dissociate at higher temperatures. To enable selections that assess not only binding affinity but also other desirable properties, such as thermostability, we chose to use the Y-ligation strategy, where the PuL and mRNA transcripts form a covalent bond. We made modifications to a previously reported PuL[29] (Figure 1B, step 2 and Table S1). We introduced a 5′-monophosphate in the oligonucleotide sequence in order to improve its ligation efficiency with 3′−OH of mRNA. Additionally, we included an internal fluorescein labeled dT into the linker region to facilitate detection of mRNA-puromycin ligation products (mRP), mRNA-puromycin-protein conjugates (mRPP), and cDNA/mRNA-puromycin-protein conjugates (mRPPD) (Figures 1B and 2A,B). A TGA stop codon was introduced behind a flexible linker to stall the ribosome at the end of the mRNA in the absence of termination factors of the defined *in vitro* translation system, facilitating the ligation of the translated protein and its mRNA-puromycin molecule (Figure 1B, step 3).

Most mRNA display systems rely on eukaryotic cell-free protein synthesis systems (CFPS), such as those derived from rabbit reticulocyte extract or wheat germ cell extract.[22,23,25] While rarely discussed explicitly, this preference is probably due to the lower nuclease activity of the eukaryotic cell extracts as well as the ability of eukaryotic ribosome to synthesize longer polypeptides.[30] Nonetheless, the *E. coli* S30 lysate-based CFPS has been used successfully in ribosome display to select libraries based on different scaffolds such as scFv fragments[31] and designed ankyrin repeat proteins (DARPins), which are particularly suitable for *in vitro* translation because of their robust folding, high stability, and absence of disulfide bonds.[32] Usually, low temperature and a high Mg^{2+} concentration are used to stabilize mRNA-protein-ribosome complexes, and the mRNA can simply be retrieved afterward by adding EDTA. However, we found that the 6-carboxyfluorescein-labeled mRNA molecule was completely degraded within 5 min in

https://doi.org/10.1021/acssensors.3c02471
ACS Sens. 2024, 9, 2846−2857

the S30 CFPS at 37 °C, rendering it unsuitable for mRNA display (Figure S1A).

While mRNA-puromycin conjugates could not be detected in the S30 CFPS, it remained intact in the PURE cell-free system that is composed of the purified translation machinery[33] (Figure S1B). RT-qPCR analysis revealed that the tested RNA was approximately 330 times more stable in the PURE system compared to S30 CFPS (Figure S1C). This is not surprising as the PURE system made of the highly purified translational machinery with the minimal nuclease and protease activities. We compared two commercially available PURE systems, PURExpress Δ*RF*123 kit and PURExpress customized kit lacking the release factors 1, 2, and 3 as well as the ribosome recycling factor. Due to the improved purification process of individual components, PURExpress has even lower RNase activity than the original PURE system. Omission of the release factors prevents the system from processing of the stop codons therefore facilitating ribosomal stalling and covalent bond formation between the mRNA-puromycin and the nascent peptide chains. The customized PURExpress exhibited a higher protein display efficiency (Figure S2D) and thus was chosen for further experiments.

To ascertain functionality of mRNA display, we closely monitored the formation of mRP, mRPP and mRPPD. By optimizing the conditions and purification protocols for each reaction (Supporting Information, Figure S2), we were able to achieve nearly 100% mRP formation efficiency as confirmed by the densitometric analysis of the mRNA and mRP bands separated on TBE-urea gel (Figure 2A). The efficiency of protein display on mRNA was estimated to be 30−40% as confirmed by quantifying both the mRNA (ratio of protein conjugated mRNA to total mRNA) and protein fractions (ratio of mRNA displayed protein to total protein) (Figure 2B and Supporting Information, Figure S2C).

We explored the use of a 2′-*O*-methylated PuL (Table S1) and investigated substitution of the TGA codon with consecutive rare codons in front of the PuL hybridization site. Contrary to earlier reports,[24,34] in our hands, these modifications did not result in significant improvements in protein display efficiency (Figure S2D,E). To streamline the selection process, we removed the purification or desalting steps and used the crude translation reaction for reverse transcription. EDTA was added after reverse transcription to facilitate ribosome dissociation before the panning step. This allows us to complete a selection round in 7 h (Supplementary text and Figure S3).

We next assessed target mRNA enrichment in each cycle of the mRNA display. To minimize selection bias, we compared mRNAs with similar reverse transcription and PCR amplification efficiencies while ensuring that the corresponding cDNAs could be distinguished by agarose gel electrophoresis. We inserted either a Flag-tag or a Twin-Strep-tag in front of the monobody domain (Mb) to allow capture and detection of translation products. When we combined mRNAs of Flag- and Twin-Strep-tagged Mb in 1:1 ratio, we observed that these two mRNAs were reverse transcribed and PCR amplified with a similar efficiency (Figure 2C). To assess enrichment efficiency, we mixed both mRNAs in different ratios (1:10, $1:10^2$, $1:10^3$, and $1:10^4$) and selected against Flag-antibody coated Dynabeads. After one round of selection, we could amplify the Flag-Mb cDNA even when its mRNA template was present in only 0.1% of the total RNA pool (Figure 2D). Subsequent selection rounds further increased the abundance of Flag-Mb cDNA (Figure S4). We concluded that in this binary model system each round of selection had an enrichment factor of approximately 10^3.

Design of Fibronectin 3-Based Binder Library. Given the multidomain structure of our biosensors, it is crucial to keep the size of the individual domains to a minimum. Hence, we chose the engineered 10th domain of fibronectin type III, termed FN3con (PDB: 4u3h), as the scaffold for our library (Figure 1C). Engineered using consensus protein design, this 87-amino acid beta-sandwich fold with seven strands connected by six loops has optimized surface electrostatics and hydrophobic packing and, as a result, displays high thermostability (Tm > 100 °C).[35] Binders selected from a library based on a stable scaffold likely preserve the scaffold's stability.[36,37] Three solvent-exposed CDR-like loops located on one side of the protein provide an interface for ligand binding. Unlike the immunoglobulin domain, FN3con is free of disulfide bonds, enabling its efficient production in expression systems that do not contain a disulfide-forming system.

We designed an FN3con-based sequence encoding an N-terminal Flag-tag, the FN3con domain, and a C-terminal GS-rich flexible linker to reduce the steric coupling between the translated protein and its mRNA. A combinatorial DNA library (Table S1 and Figure 1B) encoding the 5′ and 3′- elements required for mRNA display, along with the FN3con domain containing three fully randomized CDRs of fixed lengths, was commercially synthesized. Each amino acid position in these regions was mutated to 18 amino acids, excluding methionine and cysteine. The theoretical diversity of the library was calculated as 10^{27} and could not be fully covered by the synthesis process. Next generation sequencing (NGS) data analysis of the library confirmed that over 65% of the products were full-length and the ratio of amino acids at each position was within 75% of the designed percentage, resulting in a library with $\sim 10^{10}$ diversity.

mRNA Display Selection of FN3con Binders against Three Human Transaminases. To test our selection platform, we choose to select binders against three human aminotransferases: cytosolic aspartate aminotransferase (cAST), mitochondrial aspartate aminotransferase (mAST), and alanine aminotransferase 1 (ALT). These proteins are used as clinical biomarkers of liver damage,[38,39] and biosensors detecting them would be of potential value in diagnostics and drug development. To ensure selective and efficient immobilization of the target proteins on a support matrix, we incorporated a 15-amino acid Avi-tag at the N-terminus of each target protein which mediates its biotinylation in *E. coli* strains coexpressing biotin ligase BirA.[40]

We performed mRNA display selections against all three biotinylated transaminases immobilized on streptavidin-coated Dynabeads. Initially, the mRPPD library (Figure 1B, step 5) was subjected to negative selection on empty beads to eliminate nonspecific binders, followed by the positive selection on transaminase-saturated beads. For the cAST protein, we performed six rounds of selection, including five rounds of surface panning and one round of solution panning, at two different cAST concentrations. In the later rounds of selection, we increased the number of washes, included high-salt washing buffer, increased incubation time with negative beads, and decreased incubation time with target-loaded beads.

Each selection round was analyzed by qPCR and polyclonal ELISA binding assays (Figure 3A,B). We observed a sharp increase in the recovered cDNA in round 4 selection that was

https://doi.org/10.1021/acssensors.3c02471
ACS Sens. 2024, 9, 2846−2857

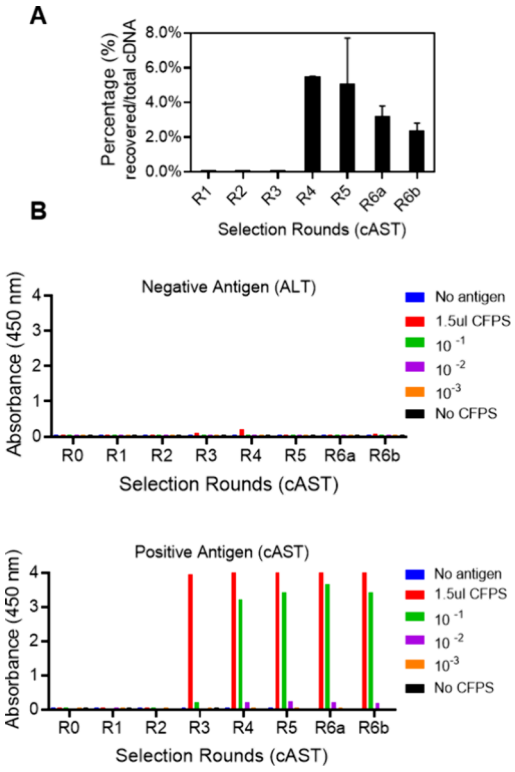

Figure 3. Analysis of a representative mRNA display selection campaign against cytosolic aspartate aminotransferase (cAST). (A) Bar plot showing the relative enrichment of FN3con cDNAs in subsequent rounds of selection against cAST as quantified by qPCR analysis of the input and output cDNA. (B) ELISA signals of the serially diluted CFPS reactions primed with a cDNA naïve library (R0) and outputs of all six rounds of selection (R1−R6). The interactions were detected using the HRP-conjugated anti-Flag antibody.

maintained in round 5. In round 6b, where a lower concentration of the target protein was used compared to R6a, we recovered less cDNA. For the ELISA assays, we immobilized either the target protein cAST or a nonrelated protein (ALT) on an ELISA plate and added the PURExfrex translation reaction programmed with cDNAs from each selection round. ELISA detection of the Flag-tag revealed that binder enrichment became evident in round 3 and further increased in rounds 4−6. Translation reactions programmed with R0, R1, or R2 cDNA resulted in no detectable signal, indicating low prevalence of cAST binders. Control wells coated with a negative antigen exhibited no signals, indicating the absence of nonspecific binders.

We subsequently performed five rounds of mRNA display selection against mAST and ALT proteins (Figure S5). In the mAST binder selection campaign, we observed a notable increase of the recovered cDNA in round 4, followed by a further increase in round 5 (Figure S5A). ELISA assays demonstrated substantial enrichment of mAST binders in both rounds 4 and round 5. However, we observed some cross-reactivity with ALT but, given the much stronger signal in the positive control, we proceeded with the selection (Figure S5B). For the ALT binder selection campaign (Figure S5C,D), a surge in recovered cDNA was observed in round 5, while the ELISA signal could be detected already in round 4. Importantly, no nonspecific binding was observed, as all negative controls produced a minimal signal.

Sequence Analysis of Putative cAST Binders. We utilized NGS to analyze cDNA pools from both the naïve library and its six selection rounds. In the naïve library, the ratio of unique sequences to the total sequences ($R_{unique/total}$) was nearly 100%, while the ratio of the frequency of most enriched sequences to the total sequences ($R_{MAXfreqency/total}$) was below 0.5% (Figure S6A,B). After the selection, the $R_{unique/total}$ decreased while the $R_{MAXfreqency/total}$ increased, indicating enrichment of binders during the selection process (Figure S6A,B). Specifically, the $R_{unique/total}$ remained very high at >98% in rounds 1 and 2, decreasing to 59% at R3, and then below 10% in rounds 4−6. At round 6a, approximately 15,000 unique sequences were present. Meanwhile, the $R_{MAXfreqency/total}$ stayed below 0.3% from round 1 to round 2, gradually increased to 8% at round 3, 24% at round 4, and further rose to 36% at round 5 and 43% at round 6. Plotting the frequency of the top 200 sequences revealed a noticeable increase in the sequences with higher frequency in the later rounds of selection (Table S2 and Figure S6C).

To visualize the sequence evolution trajectories throughout the selection campaigns, we generated a bump chart, using the top 20 sequences from the first round (R1) and the last round (R6b) as anchor points (Figure S6D). Analysis of the chart indicated that one or two selection rounds, combined with NGS sequencing, might be sufficient to identify specific binders. However, physical isolation of these binders is difficult due to their low frequencies in the earlier rounds and therefore additional enrichment rounds are required.

Biophysical Characterization of Putative cAST Binding Domains. To characterize the selected binders, we cloned cDNA from round 5 of cAST binder selection into a pET28a expression vector in frame with an N-terminal His-tag and a C-terminal calmodulin binding peptide (CaM-BP) and subjected individual clones to Sanger sequencing. Out of 51 single colonies with reliable Sanger sequencing results, we identified three clones that had more than one sequence (Table S3). We include these sequences (cB1-CaM-BP, cB2-CaM-BP, cB7-CaM-BP) as well as seven other sequences with a unique Sanger sequence but with high frequencies (>1%) in NGS data (cB3-CaM-BP, cB4-CaM-BP, cB5-CaM-BP, cB6-CaM-BP, cB8-CaM-BP, cB9-CaM-BP, cB10-CaM-BP) for further investigation. We expressed these proteins in *E. coli* and purified them to near homogeneity using Ni-NTA affinity chromatography (Figure S7A). Semiquantitative ELISA was used to estimate the binding affinity of purified proteins for the cAST protein, revealing apparent K_d values in a range of 2−15 nM (Figure S8). For cB10-CaM-BP, we corroborated these findings using biolayer interferometry (BLI) leading to a K_d value of 2.4 ± 0.04 nM, with a k_{on} of 3.1×10^5 M^{-1} $s^{-1}$and a k_{off} of 3.2×10^{-4} s^{-1} (Figure S13).

Construction and Testing of cAST Biosensors. To evaluate the suitability of the isolated binder domains for constructing protein biosensors, we cloned five cAST binders into an expression vector in frame with an N-terminal TEM-1 β-lactamase-calmodulin chimera switch module (BLA-CaM)[15] and a C-terminal His-tag (Table S1). The activity of this sensor can be monitored by a chromogenic substrate, such as nitrocefin (Figure 1A). We produced the recombinant proteins in *E. coli* and purified them in near homogeneity (Figure S7A). The functionality of BLA-CaM-binder fusions was assessed by incubating them to M13 CaM-Binding peptide, which binds to and activates the biosensor core (Figure S9).[41] All fusion

https://doi.org/10.1021/acssensors.3c02471
ACS Sens. 2024, 9, 2846−2857

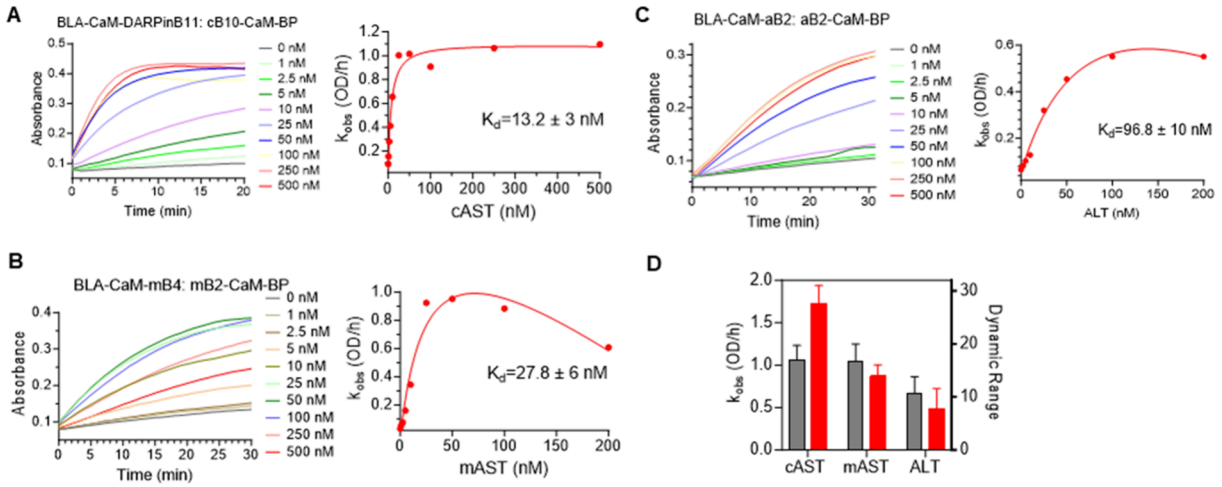

Figure 4. Performance analysis of the developed two-component biosensors for three transaminases. (A) Titration of cAST to a solution of 25 nM BLA-CaM-DARPinB11 and 100 nM cB10-CaM-BP. The change in absorption of nitrocefin was recorded over 20−30 min, and the linear phase of reaction was used to derive k_{obs}. The k_{obs} values were plotted against the cAST concentration and fitted using nonlinear regression to calculate the apparent K_d. (B) Titration of a 25 nM solution of BLA-CaM-mB4 and 100 nM mB2-CaM-BP was performed with increasing concentrations of mAST. (C) Titration of a 25 nM solution of BLA-CaM-aB2 and 100 nM aB2-CaM-BP with increasing concentrations of ALT. The experiments in (A−C) were conducted at least twice, with representative kinetics data shown and K_d values presented as mean ± SD. The hook effect was observed when the analytes were added to the assay at high concentrations. (D) Plot of maximal k_{obs} (gray bars) and dynamic ranges (red bars) for the three best transaminase biosensors from (A−C). Error bars were calculated based on two experimental replicates.

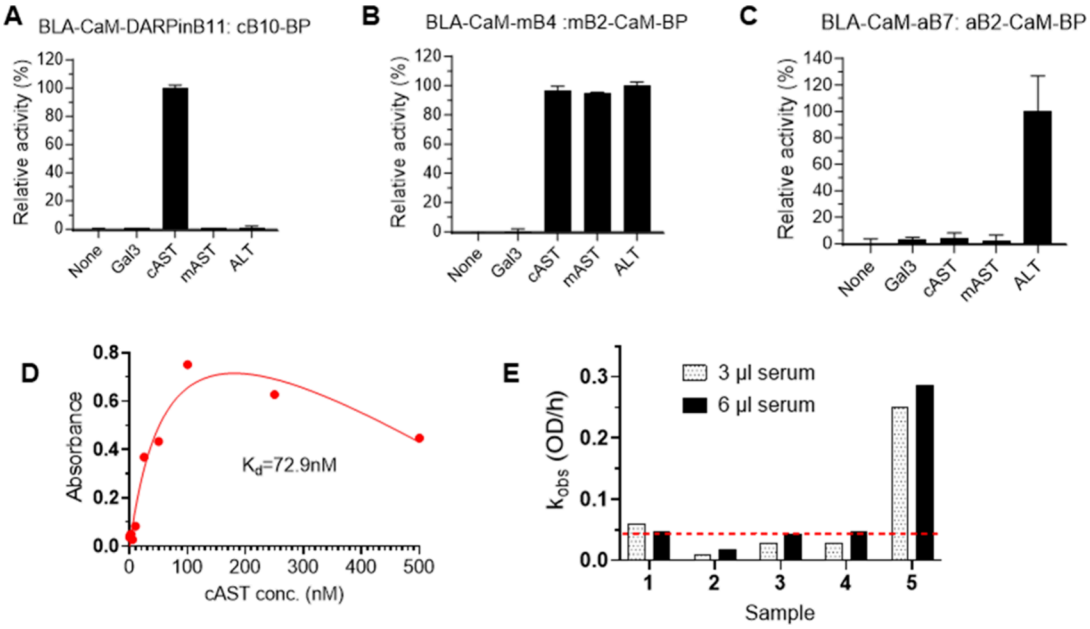

Figure 5. Specificity analysis and performance in human serum of the developed two-component biosensors. (A) Relative activity of the cAST biosensor in the presence of different proteins. The assays were performed in a buffer containing 25 nM BLA-CaM-DARPinB11 and 100 nM cB10-CaM-BP with or without 200 nM analyte protein. After addition of nitrocefin to a final concentration of 50 μM, the progression of the reaction was monitored for 30 min. The linear phase of the reaction was used to derive k_{obs}, and the relative activity was calculated as the ratio of k_{obs} compared to the one against its target protein. (B) As in (A) but for the mAST biosensor containing 25 nM BLA-CaM-mB4 and 100 nM of mB2-CaM-BP. (C) As in (A) but for the ALT biosensor containing 25 nM of BLA-CaM-aB2 and 100 nM of aB2-CaM-BP. (D) Titration of cAST biosensors with recombinant cAST protein in the presence of 6 μL of control serum using 25 nM BLA-CaM-DARPinB11 and 100 nM of cB10-CaM-BP. (E) Detecting cAST in patient sera. Five serum samples were spiked at either 3 μL or 6 μL into the biosensor assay. Sample 1 represents the control serum with a cAST level of <5 U/L (corresponding to <1.4 nM); samples 2, 3, 4, and 5 correspond to serums with cAST levels at 22, 118, 486, and 4360 U/L, respectively.

proteins displayed M13 CaM-BP-dependent activation, albeit with different maximal catalytic activities.

Next, we tested activities of different combinations of BLA-CaM-binder fusions with binder-CaM-BP fusions in the absence and presence of cAST and identified the BLA-CaM-cB10/cB10-CaM-BP combination as the best performing pair (Figure S10). This is made possible by the homodimeric structure of cAST that mediates assembly of biosensor components with identical binders.[44] We titrated cAST into the mixture and used the k_{obs} rates of catalytic turnover to

https://doi.org/10.1021/acssensors.3c02471
ACS Sens. 2024, 9, 2846−2857

estimate the apparent K_d of this biosensor for cAST as 251 nM with a dynamic range of 7-fold (Figure S11).

Additionally, we produced biosensor pairs that utilized DARPins[42] as binding domains against cAST, which were selected using ribosome display methods described previously (Supplementary text and Table S4).[43,44] The best-performing combination, BLA-CaM-DARPinB11/DARPinB11-CaM-BP, displayed an apparent K_d value of 64.3 nM and a dynamic range of 13-fold (Figure S11). We also investigated DARPin fusions with BLA-CaM in combination with FN3con-based cAST binders fused to CaM-BP (Figure S10). The best identified combination was BLA-CaM-DARPinB11 with cB10-CaM-BP, which has an apparent K_d of 13.2 nM and a dynamic range of 28-fold (Figure 4A,D). The large dynamic range of this combination points to a potential benefit of combining different scaffolds in this biosensor design to achieve optimal biosensor performance.

Streamlining mAST and ALT Biosensor Development. To streamline the biosensor construction and characterization procedure (Figure S12), we cloned cDNAs of FN3con selected against mAST in frame with the CaM-BP and BLA-CaM protein, respectively. Sequence analysis of the clones led to the identification of four sequences of putative mAST binders in both CaM-BP and BLA-CaM constructs (Table S3). We were able to express and purify all corresponding proteins except BLA-CaM-mB3 (Figure S7B). The combinatorial biosensor assay identified the BLA-CaM-mB4/mB2-CaM-BP pair as the best combination, with an apparent K_d for mAST of 28 nM and a dynamic range of 9-fold (Figure 4B,D). We applied the same approach to putative ALT binders and generated five CaM-BP fusions and five BLA-CaM fusions (Table S3 and Figure S7C). The biosensor assay identified the best combination as BLA-CaM-aB2/aB2-CaM-BP, which has an apparent K_d value for ALT of 97 nM and a dynamic range of 8-fold (Figure 4C,D). Interestingly, the performance of the biosensors varied in regard to the high dose hook effect[45] where the biosensor with the combination of DARPinB11 and cB10 binders maintained its activity even at high concentrations of cAST (Figure 4A). This is in contrast to the biosensors with other binder combinations that displayed significant inhibition at high analyte concentrations. This may indicate that DARPinB11 and cB10 binders act cooperatively, where the first binding event increases the affinity of the target for the second binder. In principle, such binders can be selected using the developed platform by performing selection of the second biner against the analyte: binder 1 complex.

We selected the best performing biosensors and measured their target binding affinity using biolayer interferometry (BLI) (Figure S13) in the format of the fusion with the CaM binding peptide. The mB2-CaM-BP and mB4-CaM-BP displayed K_d values of 7.1 ± 0.095 and 13 ± 0.3 nM, respectively, toward mAST. Notably, mB4-CaM-BP exhibited a faster k_{on} and faster k_{off} compared to mB2-CaM-BP. In the case of ALT binder, aB2-CaM-BP demonstrated a high affinity for ALT, with a K_d value of 2.7 ± 0.04 nM. Additionally, the k_{on} and k_{off} values were measured as 3.0×10^5 M^{-1} s^{-1} and 5.7×10^{-4} s^{-1}, respectively. These results confirm that the combinatorial assay could be used to identify binders optimally performing in the biosensor context.

Analysis of Biosensor's Specificity and Performance in Clinical Samples. We evaluated the specificity of the developed biosensors toward all three transaminases and a nonrelated protein, galectin-3 (Figure 5). As expected, none of the sensors responded to galectin-3, demonstrating their selectivity. Both the cAST and ALT biosensors displayed excellent specificity and did not show any reactivity toward the other transaminases. However, the mAST biosensor unexpectedly reacted with all three transaminases. This cross-reactivity is probably due to the low specificity of selected mAST binders. Although we did not characterize the binding of individual mAST binders, we do observe nonspecific binding of the selected mAST binder pools from mRNA display campaign to other transaminases (Figure S5B). Despite the relatively low degree of sequence similarity among these transaminases, they share the same tertiary fold, which might explain the observed cross-reactivity. This highlights the importance of implementing a more rigorous counterselection step during the selection process.

The top-performing cAST biosensor exhibited a limit of detection (LOD) of 0.64 nM, which is significantly below the normal cAST serum concentration of 2.7−11 nM. We therefore decided to test the ability of the developed two-component biosensor to detect cAST in serum samples. First, we spiked serially diluted cAST protein into the control serum to assess the biosensor's performance in that medium. We observed that the serum affected the enzymatic activity of the biosensor, making the cAST concentration below 10 nM undetectable (Figure 5D). Next, we used our biosensor assay to analyze patient samples with cAST concentrations ranging from <1.4 (5U/L) (control serum) to 1200 nM (4360 U/L). While the biosensor reliably detected the cAST concentration in the 10−100 nM range, concentrations below 10 nM could not be quantified (Figure 5E). Further optimization of the biosensor assay together with affinity maturation will be necessary to increase assay sensitivity and endow it with clinical utility.

DISCUSSION

Here, we present a pipeline for construction of two-component allosteric biosensors based on reporter-calmodulin chimeras.[9,15] Previously, we constructed such biosensors using binders from structures deposited in the PDB database. To address the obvious limitation of this approach, we employed mRNA display to enable the rapid development of protein binders and their testing in the context of the two-component biosensor architecture. To reduce the complexity of the selection process and increase its throughput, we systematically optimized each step in the mRNA display. The optimized protocol enabled us to achieve the display efficiency at least 2-fold higher than previously reported[24] and to complete a selection round in a single day. While a faster time line was previously reported for the PURE-based mRNA selection system, it relied on a noncovalent linkage of mRNA and its product, thereby limiting the experimental conditions under which the selection can be performed.[24] We successfully obtained high affinity FN3con binders for all three tested protein targets, enabling the construction of protein biosensor candidates within weeks. We demonstrated that a focused library of binding domains fused with biosensor components allowed rapid identification of optimal biosensor combinations.

The three human transaminases investigated here form homodimers,[46] which, in principle, allows for the use of the same binding domain for both elements of a two-component biosensor (Figure 4C and Figure S11). If this is not the case, binder pairs with nonoverlapping epitopes have to be identified. Furthermore, we also used ribosome display to

https://doi.org/10.1021/acssensors.3c02471
ACS Sens. 2024, 9, 2846−2857

select DARPins and demonstrated that combination of FN3con and DARPins binders yields very well performing sensors. This is in line with what has been reported for other biosensor architectures, where the combination of different binders also gave the best performance.[47]

During the establishment of our binder development pipeline, we compared two sequencing strategies to analyze the enriched sequences. Initially, we conducted five to six rounds of selection and then subjected cDNAs to Sanger sequencing, limiting the sampling depth to 100. Prior to round 5, we rarely recovered multiple copies of the same binders. NGS sequencing allowed us to track the sequence evolution trajectory more effectively. Interestingly, we found that most of the top 20 sequences from round 5 or round 6 were present at round 1 but with much lower frequencies (Figure S6D). This suggests that one or two selection rounds combined with NGS sequencing may be sufficient to identify the most promising binders. It is noteworthy that even in the round 6, the enriched library still contained $>10^3$ unique sequences that cannot be effectively sampled by the presented biosensor development approach. However, it points to the lack of "library focusing"[19] in the *in vitro* display methods such as mRNA and ribosome display, as opposed to *in vivo* methods such as phage or yeast displays. The abundance of candidate binders calls for biosensor testing methods with a higher throughput. In principle, the use of a β-lactamase reporter may enable antibiotic resistance-based selection approaches.

Testing of the developed pipeline allowed us to identify the further challenges associated with developing new protein biosensors. We observed a discrepancy between the K_d values measured by ELISA or bilayer interferometry and the apparent K_ds determined in the biosensor assay (Table S6). This is not entirely surprising, since in the context of a two-component biosensor other factors such as binder orientation, kinetic parameters, and the overall avidity of the system are likely to play a role. This strongly suggests that the biosensor construction process should not rely solely on the binding affinity. Given the biosensor's functional mechanism, the best scenario implies that the two binding domains in the sensor should associate with two independent sites on the target, which can also correspond to equivalent sites in a homodimeric target, and that their positions and orientation should allow optimal interaction of the calmodulin switch with its ligand peptide CaM-BP. However, in the absence of structural information, optimization of these parameters is not possible, and hence, combinatorial testing of many variants may be required. Given the advancements in protein and protein:protein interaction modeling, computational methods may help to more effectively rank binders emerging in selection rounds.

Another learning from the presented experiments was about the role of epistatic interactions within biosensor assemblies. While the employed system is modular, it is based on a fusion of multiple elements into a single polypeptide chain that interacts with each other both thermodynamically and kinetically. The ability to quantify the catalytic activity of the core switch by exposing the fusion to a calmodulin-binding peptide allowed us to assess the epistatically induced variability of the generated sensors. These results demonstrated that the activity of these fusion modules varied up to 28 times (Figure S10). When a BLA-CaM-Binder fusion was tested against several Binder-CaM-BP, we observed a much smaller variation in activity (1.8−3.1 times), indicating a small epistatic effect. Given the large influence of the binder domain sequence on the reporter's activity, the optimal strategy appears to be to select chimeras with optimal catalytic rate and affinity for the target and then test them against a library of Binder-CaM-BP fusions to identify combinations with the optimal performance.

We demonstrated that developed cAST biosensors could detect cAST in clinical samples, albeit only in patient samples with high biomarker concentrations. One way to enhance the biosensor's sensitivity is to further improve its affinity through maturation using the error-prone PCR,[48] DNA shuffling,[49] and DIMPLE (deep insertion, deletion, and missense mutation).[50]

MATERIALS AND METHODS

Materials. The sequences of oligonucleotides, gBlocks, and the parental combinatorial FN3con DNA library used in this work are listed in Table S1 of the Supporting Information. These were purchased from either Bioneer Pacific, Integrated DNA Technologies (IDT), Gene Universal, or Twist as indicated in Table S1. The fluorescently labeled oligonucleotides were commercially synthesized and HPLC-purified by IDT Inc. (Coralville, USA). Chemicals were purchased from Sigma unless otherwise indicated.

Preparation of FN3con Library for mRNA Display Selection. The combinatorial DNA library encoding the 5′ and 3′-elements required for the mRNA display of a Flag-tagged FN3con domain (PDB: 4u3h) with three fully randomized CDRs was synthesized by Twist. The sequence of the parental template is provided in Table S1. The nucleotides corresponding to the amino acids in the loop regions (CDR1/CDR2/CDR3:EPPPGPIT/PGSETS/NGAGEGPP) were randomized to 18 amino acids (except Cys and Met), and stop codons were excluded. The synthesized DNA library was verified using NGS at Twist and provided at a 20 μg scale. The DNA library was then amplified using a PCR reaction containing 1× NH_4 buffer (Bioline), 0.2 mM dNTPs (Thermo Fisher Scientific), 2 mM $MgCl_2$ (NEB), 2 nM pfux7 DNA polymerase,[51] 0.25 μM primer 54, and 0.25 μM primer 64 (Table S1). The PCR program included an initial denaturation at 95 °C for 1 min, followed by 8 cycles of denaturation at 95 °C for 30 s, annealing at 70 °C for 30 s, extension at 72 °C for 30 s, and a final extension step at 72 °C for 5 min. The PCR product was purified using the Wizard SV Gel and PCR clean-up system (Promega) according to the manufacturer's instruction.

Subsequently, the DNA library was transcribed into the mRNA library in 40 mM Hepes-KOH (pH 7.9), 25 mM $Mg(OAc)_2$, 2 mM spermidine, 40 mM DTT, 5 mM rNTPs, 50 μg/mL T7 RNA polymerase, 50 μg/mL yeast inorganic pyrophosphatase, and ∼20 ng/μL DNA template at 35 °C for 3 h. After digestion of the DNA template using DNaseI (NEB), the transcribed mRNA library was purified using the Monarch RNA Cleanup Kit (NEB). The resulting naïve FN3con library was separated on a preparative 6% Urea-PAGE gel and stained using SYBR Safe (Thermo Fisher Scientific). The correct size band was excised from the gel and crushed into small pieces for further purification using the Electro-Eluter (Model 422, BioRad). The recovered mRNA library was dissolved in RNase-free water and stored at −80 °C.

To introduce the puromycin oligonucleotide into the mRNA library, ligation was performed at 37 °C for 30 min. The ligation reaction contained 40 mM Hepes buffer (pH 8.2), 18 mM Mg^{2+} ($MgCl_2$:$Mg(OAc)_2$ = 1:1), 5% PEG 8000, 2 mM ATP, 4 μM mRNA, 5 μM puromycin oligonucleotide (PuL, Table S1), 1 mM DTT, 0.15 U/ μL T4 RNA ligase 1 (Epicenter), and 0.2 U/ μL RNaseOUT (Invitrogen). The ligated mRNA-PuL conjugate was then purified using Monarch RNA cleanup kit (NEB), eluted in RNase-free water and stored at −80 °C.

Model Selection and Estimation of the Enrichment Factor in each mRNA Display Selection Round. The Flag-Mb (gB1) and Twin-Strep-Mb (gB2) DNA templates were synthesized as gBlocks (Table S1) and amplified using the specific primer pairs, 102 and 64 and 103 and 64, respectively. The PCR was carried out as described above; however, an annealing temperature of 60 °C and 30 cycles of

https://doi.org/10.1021/acssensors.3c02471
ACS Sens. 2024, 9, 2846−2857

amplification were used. Following PCR, the purified DNA was subjected to *in vitro* transcription and DNAaseI treatment to obtain the corresponding RNA, which was subsequently purified and ligated with puromycin oligonucleotide, as described above.

The resulting mRNA-puromycin conjugates, Flag-Mb-PuL and Twin-Strep-Mb-PuL, were mixed at different ratios, as indicated in Figure 2D. A 1 μM mixture of the conjugates was translated using 4 μL of PURExpress Δ*RF*123 Kit (NEB) at 37 °C for 30 min. Next, 4 μL of $MgCl_2$/KCl (750 mM KCl and 65 mM $MgCl_2$) was added, and the reaction mixture was incubated at 37 °C for 20 min. The reaction was terminated by adding 42 μL of 50 mM Tris-acetate (pH 8.2) and 20 mM EDTA and thoroughly mixed. The mRNA-protein complex was purified using the Monarch RNA cleanup kit (NEB) and eluted in 6.5 μL RNase-free water. The collected sample was then used to set up a 10 μL reverse transcription reaction using the SuperScript III First-Strand Synthesis System (Thermo Fisher Scientific) with primer 64. After incubation at 42 °C for 20 min, 1 μL of the reverse transcribed product was reserved for qPCR-based quality control, and the remaining 9 μL were diluted with 27 μL HBST buffer containing 50 mM Hepes-KOH (pH7.5), 300 mM NaCl, and 0.05% (v/v) Tween 20. To this mixture, 0.3 μL of biotinylated Flag-tag monoclonal antibody (Thermo Fisher Scientific) was added to a final concentration of 50 nM. The mixture was incubated at room temperature for 30 min, followed by the addition of 5 μL of Streptavidin Dynabeads M280 or C1 (Thermo Fisher Scientific), and further incubated at room temperature for 15 min. The Dynabeads were then washed four times with 200 μL of PBST. During the final wash, the content was transferred to a new tube. The cDNA was eluted using 36 μL of 0.5 × PCR buffer (5 mM Tris-HCl, pH 8.4, 25 mM KCl, 0.05% Triton X-100) at 95 °C for 5 min. qPCR was subsequently performed using primer pair 54/64 and SsoAdvanced Universal SYBR Green Supermix (BioRad). The PCR products were then separated on a 2% agarose gel to assess the ratio of the two cDNA products.

mRNA Display Binder Selection against cAST. The naïve mRNA library was ligated to PuL and purified by using the Monarch RNA cleanup kit. Subsequently, the mRNA-PuL conjugate was translated at a final concentration of 1 μM using a customized PUREfrex 1.0 kit (Δ*RF*1, RF2, RF3, RRF, and COSMO BIO Co. Ltd.) in a total volume of 100 μL at 37 °C for 50 min. The translation reaction was then used to set up a reverse transcription reaction using the SuperScript III First-Strand Synthesis System (Thermo Fisher Scientific) with primer 64 at 42 °C for 20 min. Eight μL of 250 mM EDTA (pH 8) was subsequently added, and the mixture was diluted 10 times by adding 800 μL of PBST buffer. Two μL of the diluted mixture was reserved for qPCR-based quality control with the rest being centrifuged at 21,000*g* for 5 min to remove any aggregates. The supernatant was then incubated with 50 μL of empty Dynabeads MyOne Streptavidin C1 (Thermo Fisher Scientific) at 20 °C for 20 min. After the Dynabeads were separated on a magnetic stand, the supernatant was incubated with 50 μL of cAST-saturated Dynabeads C1 for 20 min. The Dynabeads were then washed four times with 1 mL of PBST buffer. After the final wash, the mixture was transferred to a new low-binding microcentrifuge tube (Costar, #3207). The Dynabeads were resuspended in 100 μL of 0.1X PCR buffer (1 mM Tris-HCl, pH 8.4, 5 mM KCl, 0.01% TritonX-100) and heated at 95 °C for 5 min. Two μL of the eluted cDNA was reserved for qPCR, while the rest was transferred into a new tube and used to set up a PCR reaction at 10× the supernatant volume using 8−12 amplification cycles. The resulting PCR products were purified using Wizard SV Gel and PCR Clean-Up System (Promega) and then eluted using 50 μL of RNase-free water. The purified cDNA was subsequently prepared for round 2 selection by performing *in vitro* transcription, DNAaseI treatment, puromycin oligonucleotide ligation as described above. The mRNA-PuL conjugate was eluted into 12 μL of RNase-free water.

For subsequent rounds of selection (R2-R5), various adjustments were implemented, including altering reaction volumes, bead quantities, incubation times, washing buffer compositions, and the number and duration of washes. The translation reaction volume and reverse transcription volume for R2−R5 were reduced to 25 and 50 μL, respectively. Negative selection was performed by incubating the supernatant with 25 μL (R2−R4) or 34 μL (R5) of empty Dynabeads for 30 min, while positive selection was performed by incubating the supernatant with 25 (R2-R4) or 17 μL (R5) of cAST-saturated Dynabeads for 15 min. The number of washes increased gradually, with 4 washes at R2, 6 at R3, 7 at R4, and 8 at R5. In R5 8 washes were used, with 4 washes using PBST only and 4 washes with PBST and 360 mM NaCl. For R6, all steps were analogous to those of R5, except that two parallel selections using solution panning were conducted. Specifically, the supernatant after incubation with empty beads was divided into two. One portion was incubated with 50 nM cAST (R6a), and the other with 2.5 nM cAST (R6b) in PBST buffer for 10 min. The cAST-binder complex was captured by incubating it with 10 μL of Dynabeads for 10 min.

ELISA Assay for Characterizing the Enrichment of Potential FN3con Binders in Each mRNA Display Selection Round. To assess the enrichment of potential binders in each selection round, an ELISA assay was performed using a Maxisorp plate (no. 442404, Thermo Fisher Scientific). Wells forming columns 2−6 and columns 8−12 were coated with control protein and antigen, respectively, at a concentration of 10 μg/mL in PBS. Columns 1 and 7 were incubated with PBS and served as negative controls. The plate was then incubated overnight at room temperature. Afterward, the coated plate was washed three times with PBST buffer (PBS plus 0.1% Tween) and blocked with 2% MPBS (PBS plus 2% skim milk) for 1 h. Simultaneously, the cDNA from each selection round was translated into protein using the PUREfrex kit at 30 °C for 3 h and subsequently blocked with 2% MPBS. Following decanting of the blocking buffer from the ELISA plate, the blocked translation reactions were added to columns 2 to 5 and columns 8 to 11 in 10-fold serial dilution. Columns 6 and 12 served as negative controls and were not incubated with the translation reaction. After a 1 h incubation, the plate was washed three times with PBST and then incubated with 100 μL of 1/5000 diluted anti-FLAG M2-peroxidase (HRP) antibody (Sigma A8592) for 1 h. Following another round of washing, 100 μL of TMB solution (no. 34028, Thermo Fisher Scientific) was added into each well. The reaction was allowed to incubate for 10 min or until the blue color sufficiently developed. Finally, the reaction was stopped using 1 M sulfuric acid, and the absorbance at 450 nM was measured using a BioTek Synergy Neo2 Reader.

NGS Deep Sequencing before and after Selection. Adapter sequences were added to the cDNAs from the FN3con naïve library (R0) and each selection round (R1-R6) of cAST binders using a similar PCR reaction as described previously. One ng/μL of cDNA template and 0.25 μM each of primers 219 and 221 were utilized. The 3-step PCR program was performed using 60 °C for annealing and 12 cycles for amplification. 50 μL of PCR product was combined with 40 μL of Agencourt AMPure XP beads for purification and subsequently eluted in 40 μL of RNase-free water. Next, index sequences were incorporated into each cDNA sample using Nextra index kit v2. Following purification by AMPURE XP beads, the concentration of the eluted cDNA was measured using a Qubit Fluorometric Quantification kit (Thermo Fisher Scientific). The purity of the cDNA was analyzed using an Agilent fragment analyzer. The cDNA NGS sequencing was performed by the Central Analytical Research Facility (CARF) at QUT on an Illumina NovaSeq platform using MiSeq Reagent Kit v2 (500-cycles).

The NGS data were analyzed using custom Python scripts. To merge the cDNA sequencing data from the R1 and R2 reads, NGmerge was utilized with the dovetail mode enabled (the -d flag). NGmerge ran concurrently with the overlapping mode, attempting to merge the reads via both analysis modes and selecting the best reads. Approximately 70−80% of the reads were successfully stitched together. The most frequent read length was exactly as expected for cAsT at 285 bp. The amplicon sequence has three randomized segments interspersed among four fixed sequences (N-to-C order: TDVTSTSVTLSW, GYRVEYREAGGEWKEVTV, YTVTGLKPG-TEYEFRVRAV, and SSVSVTT); our code parsed the sequences between adjacent fixed sequences as the randomized segments.

https://doi.org/10.1021/acssensors.3c02471
ACS Sens. 2024, 9, 2846−2857

Frequencies were then tabulated to enable ratio calculations and interround changes of the parsed randomized segments.

Biosensor Assay. The functionality of the BLA-CaM-binder proteins were assessed at a concentration of 25 nM in a β-lactamase enzymatic assay. The assay was conducted in a buffer containing 20 mM Tris-HCl (pH 7.2), 100 mM NaCl, 1 mM $CaCl_2$, and 200 nM M13 CaM-BP. After adding 50 μM nitrocefin as the substrate, the reaction was monitored at 486 nm using a Neo2 plate reader. During the initial screening for the identification of the best pair of BLA-CaM-Binder/Binder-CaM-BP, a 96-well plate set up was used. The assay was performed in 20 mM Tris-HCl (pH 7.2), 100 mM NaCl and 1 mM $CaCl_2$, 25 nM BLA-CaM-binder, and 100 nM Binder-CaM-BP, with or without 200 nM transaminase protein. The reaction was monitored after adding the nitrocefin substrate.

To determine the functional affinity (K_d) value of the biosensors against their respective ligands, ligand titration experiments were conducted. The enzymatic assays were carried out as described above with the addition of varying concentrations of transaminase proteins ranging from 0 to 500 nM. The slope of the initial linear phase of the reaction was defined as k_{obs}. The k_{obs} data was plotted against the concentration of the target and then fitted to the following equation using GraphPad Prism to calculate the K_d:

$$Y = B_{max} \times X/(K_d + X) + NS \times X + Background$$

In this equation, B_{max} represents the maximum specific binding in the same units as k_{obs}. NS denotes the slope of nonspecific binding, and Background indicates the amount of nonspecific binding observed without any target addition.

The dynamic range of biosensors was calculated as the ratio of k_{obs} at the saturating ligand concentration to k_{obs} in the absence of ligand. To calculate the biosensor's limit of detection (LOD), the linear range from the titration curve was extracted and a linear regression curve was obtained to determine the standard deviation of the response (s.d.) and the slope of the calibration curve (S). The LOD was then calculated as three times the standard deviation (s.d.) divided by the slope (S).

■ ASSOCIATED CONTENT

Supporting Information

The Supporting Information is available free of charge at https://pubs.acs.org/doi/10.1021/acssensors.3c02471.

Sequences of oligonucleotides, gBlocks, parental combinatorial FN3con DNA library template, top 200 sequences identified from naïve library as well as all the six rounds selection for cAST protein, summary of enriched sequences from the mRNA display selection campaigns of all three transaminases, enriched sequences from the ribosome display selection campaign against cAST; supplementary methods including the following: molecular cloning, expression, and purification of transaminase proteins, streamlining the mRNA display pipeline, mRNA display binder selection against mAST and ALT, cloning of the binders into expression vectors in fusion with CaM binding peptide (CaM-BP) and BLA-CaM protein, recombinant expression and purification of the potential FN3con binders, K_d estimation using ELISA assay, biolayer interferometry assay, ribosome display of DARPin library and identification of cAST binders; and supplementary figures containing information regarding the mRNA display pipeline establishment, optimization and characterization, characterization of the mRNA display selection campaign, NGS data analysis, SDS-PAGE gels of all the developed sensor proteins, and scheme of the streamlined biosensor development pipeline as well as binding and functional data (PDF)

(XLSX)

■ AUTHOR INFORMATION

Corresponding Author

Kirill Alexandrov − *ARC Centre of Excellence in Synthetic Biology, Brisbane, Queensland 4001, Australia; Centre for Agriculture and the Bioeconomy and School of Biology and Environmental Science, Queensland University of Technology, Brisbane, Queensland 4001, Australia;* orcid.org/0000-0002-0957-6511; Email: kirill.alexandrov@qut.edu.au

Authors

Zhenling Cui − *ARC Centre of Excellence in Synthetic Biology, Brisbane, Queensland 4001, Australia; Centre for Agriculture and the Bioeconomy and School of Biology and Environmental Science, Queensland University of Technology, Brisbane, Queensland 4001, Australia*

Cagla Ergun Ayva − *Centre for Agriculture and the Bioeconomy and School of Biology and Environmental Science, Queensland University of Technology, Brisbane, Queensland 4001, Australia*

Yi Jin Liew − *CSIRO Health & Biosecurity, Westmead, New South Wales 2145, Australia*

Zhong Guo − *ARC Centre of Excellence in Synthetic Biology, Brisbane, Queensland 4001, Australia; Centre for Agriculture and the Bioeconomy and School of Biology and Environmental Science, Queensland University of Technology, Brisbane, Queensland 4001, Australia*

Roxane Mutschler − *Centre for Agriculture and the Bioeconomy and School of Biology and Environmental Science, Queensland University of Technology, Brisbane, Queensland 4001, Australia;* orcid.org/0009-0009-2376-4293

Birgit Dreier − *Department of Biochemistry, University of Zurich, Zurich CH-8057, Switzerland*

Maria M Fiorito − *Centre for Agriculture and the Bioeconomy and School of Biology and Environmental Science, Queensland University of Technology, Brisbane, Queensland 4001, Australia*

Patricia Walden − *Centre for Agriculture and the Bioeconomy and School of Biology and Environmental Science, Queensland University of Technology, Brisbane, Queensland 4001, Australia*

Christopher B Howard − *Australian Institute for Bioengineering and Nanotechnology, The University of Queensland, Brisbane, Queensland 4072, Australia;* orcid.org/0000-0001-9797-8686

Fernanda Ely − *Maltexco S.A, Talagante 9680086,, Chile*

Andreas Plückthun − *Department of Biochemistry, University of Zurich, Zurich CH-8057, Switzerland;* orcid.org/0000-0003-4191-5306

Carel Pretorius − *Department of Chemical Pathology, Pathology Queensland, Brisbane, Queensland 4006, Australia; Faculty of Health and Behavioural Sciences, The University of Queensland, Brisbane, Queensland 4072, Australia*

Jacobus PJ Ungerer − *Department of Chemical Pathology, Pathology Queensland, Brisbane, Queensland 4006, Australia; Faculty of Health and Behavioural Sciences, The University of Queensland, Brisbane, Queensland 4072, Australia*

https://doi.org/10.1021/acssensors.3c02471
ACS Sens. 2024, 9, 2846−2857

Ashley M Buckle − *PTNG Consulting, Melbourne, Victoria 3000, Australia;* Present Address: Present address: Replay, 5555 Oberlin Drive, San Diego CA 92121, US (A.M.B.)

Complete contact information is available at: https://pubs.acs.org/10.1021/acssensors.3c02471

Author Contributions

K.A. and Z.C. conceptualized and designed this study. Z.C., A.B., and K.A. designed the FN3con mRNA display library. Z.C. optimized the mRNA display pipeline, performed the selections, constructed, and screened the biosensor. B.D. and A.P. designed and performed ribosome display of DARPins. C.E.A. and Z.G. designed and integrated the DARPin binder into biosensor format. Y.J.L. analyzed the NGS data. Z.C., R.M., and M.M.F. produced and purified the sensor proteins. Z.G, P.W., and F.E. designed and produced the transaminase proteins. Z.C. and C.H. performed the BLI binding assay. C.P. and J.U. provided and quantified the biomarkers in the human serum samples. Z.C. and K.A. wrote the initial manuscript. R.M. edited the M & M and SI sections. All authors subsequently reviewed and/or edited the manuscript.

Funding

This work was supported in part by the Australian Research Council Discovery Projects DP160100973, DP150100936 as well as ARC Centre of Excellence in Synthetic Biology CE200100029 to KA. This work was also in part supported by HFSP grant RGP0002/2018 to KA. KA gratefully acknowledges financial support of CSIRO-QUT Synthetic Biology Alliance and CSIRO Future Science Platform in Synthetic Biology.

Notes

The authors declare no competing financial interest.

■ ACKNOWLEDGMENTS

We thank Victoria Coyne for her assistance in NGS library preparation, sequencing and data collection. The NGS data were generated by use of the Central Analytical Research Facility hosted by the Institute for Future En-vironments at QUT. We thank Dr. Hebatalla Mohamed, for her assistance with protein purification. We also thank Sven Furler, Thomas Reinberg and Joana Marinho for the High-Throughput-DARPin selection at the laboratory of Andreas Plückthun, University of Zurich, Department of Biochemistry, Switzerland.

■ REFERENCES

(1) Pawson, T. Protein modules and signalling networks. *Nature* **1995**, *373* (6515), 573−580.
(2) Stein, V.; Alexandrov, K. Synthetic protein switches: design principles and applications. *Trends Biotechnol* **2015**, *33* (2), 101−110.
(3) Jackson, C.; Anderson, A.; Alexandrov, K. The present and the future of protein biosensor engineering. *Curr. Opin Struct Biol.* **2022**, *75*, No. 102424.
(4) Nasu, Y.; Shen, Y.; Kramer, L.; Campbell, R. E. Structure- and mechanism-guided design of single fluorescent protein-based biosensors. *Nat. Chem. Biol.* **2021**, *17* (5), 509−518.
(5) Wongso, D.; Dong, J.; Ueda, H.; Kitaguchi, T. Flashbody: A Next Generation Fluobody with Fluorescence Intensity Enhanced by Antigen Binding. *Anal. Chem.* **2017**, *89* (12), 6719−6725.
(6) Ravalin, M.; Roh, H.; Suryawanshi, R.; Kumar, G. R.; Pak, J. E.; Ott, M.; Ting, A. Y. A Single-Component Luminescent Biosensor for the SARS-CoV-2 Spike Protein. *J. Am. Chem. Soc.* **2022**, *144* (30), 13663−13672.
(7) Guo, Z.; Smutok, O.; Johnston, W. A.; Ayva, C. E.; Walden, P.; McWhinney, B.; Ungerer, J. P. J.; Melman, A.; Katz, E.; Alexandrov, K. Circular Permutated PQQ-Glucose Dehydrogenase as an Ultra-sensitive Electrochemical Biosensor. *Angew. Chem., Int. Ed. Engl.* **2022**, *61* (6), e202109005.
(8) Guo, Z.; Parakra, R. D.; Xiong, Y.; Johnston, W. A.; Walden, P.; Edwardraja, S.; Moradi, S. V.; Ungerer, J. P. J.; Ai, H. W.; Phillips, J. J.; Alexandrov, K. Engineering and exploiting synthetic allostery of NanoLuc luciferase. *Nat. Commun.* **2022**, *13* (1), 789.
(9) Guo, Z.; Johnston, W. A.; Whitfield, J.; Walden, P.; Cui, Z.; Wijker, E.; Edwardraja, S.; Retamal Lantadilla, I.; Ely, F.; Vickers, C.; et al. Generalizable Protein Biosensors Based on Synthetic Switch Modules. *J. Am. Chem. Soc.* **2019**, *141* (20), 8128−8135.
(10) Guo, Z.; Smutok, O.; Johnston, W. A.; Walden, P.; Ungerer, J. P. J.; Peat, T. S.; Newman, J.; Parker, J.; Nebl, T.; Hepburn, C.; et al. Design of a methotrexate-controlled chemical dimerization system and its use in bio-electronic devices. *Nat. Commun.* **2021**, *12* (1), 7137.
(11) Quijano-Rubio, A.; Yeh, H. W.; Park, J.; Lee, H.; Langan, R. A.; Boyken, S. E.; Lajoie, M. J.; Cao, L.; Chow, C. M.; Miranda, M. C.; et al. De novo design of modular and tunable protein biosensors. *Nature* **2021**, *591* (7850), 482−487.
(12) Elledge, S. K.; Zhou, X. X.; Byrnes, J. R.; Martinko, A. J.; Lui, I.; Pance, K.; Lim, S. A.; Glasgow, J. E.; Glasgow, A. A.; Turcios, K.; et al. Engineering luminescent biosensors for point-of-care SARS-CoV-2 antibody detection. *Nat. Biotechnol.* **2021**, *39* (8), 928−935.
(13) Guo, Z.; Murphy, L.; Stein, V.; Johnston, W. A.; Alcala-Perez, S.; Alexandrov, K. Engineered PQQ-Glucose Dehydrogenase as a Universal Biosensor Platform. *J. Am. Chem. Soc.* **2016**, *138*, 10108 DOI: 10.1021/jacs.6b06342.
(14) Stein, V.; Alexandrov, K. Protease-based synthetic sensing and signal amplification. *Proc. Natl. Acad. Sci. U. S. A.* **2014**, *111* (45), 15934−15939.
(15) Guo, Z.; Smutok, O.; Ayva, C. E.; Walden, P.; Parker, J.; Whitfield, J.; Vickers, C. E.; Ungerer, J. P. J.; Katz, E.; Alexandrov, K. Development of epistatic YES and AND protein logic gates and their assembly into signalling cascades. *Nat. Nanotechnol.* **2023**, *18*, 1327 DOI: 10.1038/s41565-023-01450-y.
(16) Mahdavi, S. Z. B.; Oroojalian, F.; Eyvazi, S.; Hejazi, M.; Baradaran, B.; Pouladi, N.; Tohidkia, M. R.; Mokhtarzadeh, A.; Muyldermans, S. An overview on display systems (phage, bacterial, and yeast display) for production of anticancer antibodies; advantages and disadvantages. *Int. J. Biol. Macromol.* **2022**, *208*, 421−442.
(17) Amstutz, P.; Forrer, P.; Zahnd, C.; Pluckthun, A. In vitro display technologies: novel developments and applications. *Curr. Opin Biotechnol* **2001**, *12* (4), 400−405.
(18) Newton, M. S.; Cabezas-Perusse, Y.; Tong, C. L.; Seelig, B. In Vitro Selection of Peptides and Proteins-Advantages of mRNA Display. *ACS Synth. Biol.* **2020**, *9* (2), 181−190.
(19) Pluckthun, A. Ribosome display: a perspective. *Methods Mol. Biol.* **2012**, *805*, 3−28.
(20) Kamalinia, G.; Grindel, B. J.; Takahashi, T. T.; Millward, S. W.; Roberts, R. W. Directing evolution of novel ligands by mRNA display. *Chem. Soc. Rev.* **2021**, *50* (16), 9055−9103.
(21) Doshi, R.; Chen, B. R.; Vibat, C. R. T.; Huang, N.; Lee, C. W.; Chang, G. In vitro nanobody discovery for integral membrane protein targets. *Sci. Rep.* **2014**, *4*, 6760.
(22) Fukuda, I.; Kojoh, K.; Tabata, N.; Doi, N.; Takashima, H.; Miyamoto-Sato, E.; Yanagawa, H. In vitro evolution of single-chain antibodies using mRNA display. *Nucleic Acids Res.* **2006**, *34* (19), No. e127.
(23) Xu, L.; Aha, P.; Gu, K.; Kuimelis, R. G.; Kurz, M.; Lam, T.; Lim, A. C.; Liu, H.; Lohse, P. A.; Sun, L.; et al. Directed evolution of high-affinity antibody mimics using mRNA display. *Chem. Biol.* **2002**, *9* (8), 933−942.
(24) Kondo, T.; Iwatani, Y.; Matsuoka, K.; Fujino, T.; Umemoto, S.; Yokomaku, Y.; Ishizaki, K.; Kito, S.; Sezaki, T.; Hayashi, G.; Murakami, H. Antibody-like proteins that capture and neutralize

SARS-CoV-2. *Sci. Adv.* **2020**, *6*, eabd3916 DOI: 10.1126/sciadv.abd3916.
(25) Roberts, R. W.; Szostak, J. W. RNA-peptide fusions for the in vitro selection of peptides and proteins. *Proc. Natl. Acad. Sci. U. S. A.* **1997**, *94* (23), 12297−12302.
(26) Nishigaki, K.; Taguchi, K.; Kinoshita, Y.; Aita, T.; Husimi, Y. Y-ligation: an efficient method for ligating single-stranded DNAs and RNAs with T4 RNA ligase. *Mol. Divers* **1998**, *4* (3), 187−190.
(27) Seelig, B. mRNA display for the selection and evolution of enzymes from in vitro-translated protein libraries. *Nat. Protoc* **2011**, *6* (4), 540−552.
(28) Ishizawa, T.; Kawakami, T.; Reid, P. C.; Murakami, H. TRAP display: a high-speed selection method for the generation of functional polypeptides. *J. Am. Chem. Soc.* **2013**, *135* (14), 5433−5440.
(29) Kawamura, A.; Münzel, M.; Kojima, T.; Yapp, C.; Bhushan, B.; Goto, Y.; Tumber, A.; Katoh, T.; King, O. N. F.; Passioura, T.; et al. Highly selective inhibition of histone demethylases by de novo macrocyclic peptides. *Nat. Commun.* **2017**, *8*, 14773.
(30) Gagoski, D.; Polinkovsky, M. E.; Mureev, S.; Kunert, A.; Johnston, W.; Gambin, Y.; Alexandrov, K. Performance benchmarking of four cell-free protein expression systems. *Biotechnol. Bioeng.* **2016**, *113* (2), 292−300.
(31) Hanes, J.; Jermutus, L.; Weber-Bornhauser, S.; Bosshard, H. R.; Pluckthun, A. Ribosome display efficiently selects and evolves high-affinity antibodies in vitro from immune libraries. *Proc. Natl. Acad. Sci. U. S. A.* **1998**, *95* (24), 14130−14135.
(32) Binz, H. K.; Amstutz, P.; Kohl, A.; Stumpp, M. T.; Briand, C.; Forrer, P.; Grutter, M. G.; Pluckthun, A. High-affinity binders selected from designed ankyrin repeat protein libraries. *Nat. Biotechnol.* **2004**, *22* (5), 575−582.
(33) Shimizu, Y.; Inoue, A.; Tomari, Y.; Suzuki, T.; Yokogawa, T.; Nishikawa, K.; Ueda, T. Cell-free translation reconstituted with purified components. *Nat. Biotechnol.* **2001**, *19* (8), 751−755.
(34) Nagumo, Y.; Fujiwara, K.; Horisawa, K.; Yanagawa, H.; Doi, N. PURE mRNA display for in vitro selection of single-chain antibodies. *J. Biochem* **2016**, *159* (5), 519−526.
(35) Porebski, B. T.; Nickson, A. A.; Hoke, D. E.; Hunter, M. R.; Zhu, L.; McGowan, S.; Webb, G. I.; Buckle, A. M. Structural and dynamic properties that govern the stability of an engineered fibronectin type III domain. *Protein Eng. Des Sel* **2015**, *28* (3), 67−78.
(36) Porebski, B. T.; Conroy, P. J.; Drinkwater, N.; Schofield, P.; Vazquez-Lombardi, R.; Hunter, M. R.; Hoke, D. E.; Christ, D.; McGowan, S.; Buckle, A. M. Circumventing the stability-function trade-off in an engineered FN3 domain. *Protein Eng. Des Sel* **2016**, *29* (11), 541−550.
(37) Chandler, P. G.; Tan, L. L.; Porebski, B. T.; Green, J. S.; Riley, B. T.; Broendum, S. S.; Hoke, D. E.; Falconer, R. J.; Munro, T. P.; Buckle, M.; et al. Mutational and biophysical robustness in a prestabilized monobody. *J. Biol. Chem.* **2021**, *296*, No. 100447.
(38) Huang, X. J.; Choi, Y. K.; Im, H. S.; Yarimaga, O.; Yoon, E.; Kim, H. S. Aspartate Aminotransferase (AST/GOT) and Alanine Aminotransferase (ALT/GPT) Detection Techniques. *Sensors* **2006**, *6* (7), 756−782.
(39) Kim, W. R.; Flamm, S. L.; Di Bisceglie, A. M.; Bodenheimer, H. C. Public Policy Committee of the American Association for the Study of Liver, D. Serum activity of alanine aminotransferase (ALT) as an indicator of health and disease. *Hepatology* **2008**, *47* (4), 1363−1370.
(40) Fairhead, M.; Howarth, M. Site-specific biotinylation of purified proteins using BirA. *Methods Mol. Biol.* **2015**, *1266*, 171−184.
(41) Blumenthal, D. K.; Takio, K.; Edelman, A. M.; Charbonneau, H.; Titani, K.; Walsh, K. A.; Krebs, E. G. Identification of the calmodulin-binding domain of skeletal muscle myosin light chain kinase. *Proc. Natl. Acad. Sci. U. S. A.* **1985**, *82* (10), 3187−3191.
(42) Pluckthun, A. Designed ankyrin repeat proteins (DARPins): binding proteins for research, diagnostics, and therapy. *Annu. Rev. Pharmacol Toxicol* **2015**, *55*, 489−511.
(43) Gut, M.; Dreier, B.; Furler, S.; Sobek, J.; Pluckthun, A.; Holland, J. P. Designed ankyrin repeat proteins for detecting prostate-specific antigen expression in vivo. *RSC Chem. Biol.* **2023**, *4* (7), 494−505.
(44) Dreier, B.; Pluckthun, A. Rapid Selection of High-Affinity Antibody scFv Fragments Using Ribosome Display. *Methods Mol. Biol.* **2018**, *1827*, 235−268.
(45) Hoofnagle, A. N.; Wener, M. H. The fundamental flaws of immunoassays and potential solutions using tandem mass spectrometry. *J. Immunol Methods* **2009**, *347* (1−2), 3−11.
(46) Davoodi, J.; Drown, P. M.; Bledsoe, R. K.; Wallin, R.; Reinhart, G. D.; Hutson, S. M. Overexpression and characterization of the human mitochondrial and cytosolic branched-chain aminotransferases. *J. Biol. Chem.* **1998**, *273* (9), 4982−4989.
(47) Strittmatter, T.; Wang, Y.; Bertschi, A.; Scheller, L.; Freitag, P. C.; Ray, P. G.; Stuecheli, P.; Schaefer, J. V.; Reinberg, T.; Tsakiris, D.; et al. Programmable DARPin-based receptors for the detection of thrombotic markers. *Nat. Chem. Biol.* **2022**, *18* (10), 1125−1134.
(48) Drummond, D. A.; Iverson, B. L.; Georgiou, G.; Arnold, F. H. Why high-error-rate random mutagenesis libraries are enriched in functional and improved proteins. *Journal of molecular biology* **2005**, *350* (4), 806−816.
(49) Stemmer, W. P. Rapid evolution of a protein in vitro by DNA shuffling. *Nature* **1994**, *370* (6488), 389−391.
(50) Macdonald, C. B.; Nedrud, D.; Grimes, P. R.; Trinidad, D.; Fraser, J. S.; Coyote-Maestas, W. DIMPLE: deep insertion, deletion, and missense mutation libraries for exploring protein variation in evolution, disease, and biology. *Genome Biol.* **2023**, *24* (1), 36.
(51) Norholm, M. H. A mutant Pfu DNA polymerase designed for advanced uracil-excision DNA engineering. *BMC Biotechnol* **2010**, *10*, 21.

https://doi.org/10.1021/acssensors.3c02471
ACS Sens. 2024, 9, 2846−2857